Geophysical Journal International

Geophys. J. Int. (2022) **231,** 459–473
Advance Access publication 2022 May 13
GJI Heat Flow and Volcanology

https://doi.org/10.1093/gji/ggac176

Thermal conductivity, density and porosity of sedimentary and metamorphic rocks from the Lower and Higher Himalaya, Western Himalaya, India

S. Eswara Rao,[1,2] Labani Ray,[1,2] Tavheed Khan[1] and G. Ravi[1]

[1] *CSIR-National Geophysical Research Institute, Hyderabad* 500007*, India. E-mai: labani@ngri.res.in*
[2] *Academy of Scientific and Innovative Research (AcSIR), Ghaziabad* 201002*, India*

Accepted 2022 April 14. Received 2022 April 5; in original form 2021 July 30

SUMMARY

Thermal conductivity at ambient conditions is a vital parameter in the determination of heat flow, thermal modelling and various geoengineering purposes. We have measured thermal conductivity in the laboratory at ambient conditions using a steady-state method on 69 samples of sedimentary and metamorphic rocks from the Western Himalaya, India, for the first time covering major lithologies of the region. Density and porosity measurements have been carried out along with petrographic and geochemical studies to characterize these rocks. The investigated rocks include sandstone, limestone, dolomitic limestone, quartzite, slate, phyllite and schist. The average thermal conductivity is found to be the highest (5.4 W m^{-1} K^{-1}) for quartzite, moderate (ranges between 3.2 and 4.2 W m^{-1} K^{-1}) for sandstone, limestone and dolomitic limestone and lowest (ranges between 2.6 and 2.9 W m^{-1} K^{-1}) for the slate, phyllite and schist. The average values of the porosity for the rocks are less than 2 per cent. The variations in thermal conductivity within each rock type more or less reflect the compositional change, rather than the porosity. The measured thermal conductivity of the sandstone and limestone is found much higher than usually observed in such rocks, while it is on the lower side in the case of quartzite, phyllite and schist. Moreover, sedimentary rocks have higher density and lower porosity than usually found in such rocks. In fact, in this region, the sedimentary rocks show a similar density to that of the metamorphic rocks. The average density in sedimentary and metamorphic rocks varies from 2590 to 2780 kg m^{-3} and 2630 to 2740 kg m^{-3}, respectively. The study region comes under the seismic gap, and several hot springs also exist here. Therefore, the obtained results will be useful in thermal modelling, which is critical for the understanding of earthquake nucleation.

Key words: Composition and structure of the continental crust; Heat flow; Asia; Heat generation and transport.

1 INTRODUCTION

Thermal conductivity of the rocks is a vital parameter in the determination of heat flow and modelling thermal structure of the Earth's crust and upper mantle (Mareschal *et al.* 2000; Ray *et al.* 2003; Roy *et al.* 2008; Forster *et al.* 2010; Podugu *et al.* 2017). It is also widely used in a variety of engineering applications, including geothermal exploration, petroleum and natural gas geology, enhanced geothermal systems, coal mine shaft exploration, borehole heat exchange, planning for geological repositories for nuclear waste disposal, constructing underground tunnels for transportation and hydroelectric projects (Birch 1950; Pigford 1982; Rybach & Pfister 1994; Goy *et al.* 1996; Rybach *et al.* 2003; SKB 2005; Ray *et al.* 2007; Rutqvist *et al.* 2008; Lawless *et al.* 2010; Feng *et al.* 2013; Balkan *et al.* 2017; Shen *et al.* 2018).

In the last few decades, it has been observed that there is a large variability in thermal conductivity for each rock type, particularly in the upper crustal rocks (Kappelmeyer & Haenel 1974; Roy *et al.* 1981; Cermak & Rybach 1982; Clauser 2006; Chopra *et al.* 2020; Ray *et al.* 2021). Studies of thermal conductivity at elevated temperatures showed that variation of thermal conductivity with depth depends strongly on the thermal conductivity at ambient conditions, that is at room temperature, irrespective of rock type (Birch & Clark 1940; Kukkonen *et al.* 1999; Ray *et al.* 2021). But, the thermal conductivity at ambient condition depends on many parameters, such as mineral composition, texture (anisotropy), porosity and pore-filling fluid type (Zoth & Haenel 1988). Thus, a detailed investigation of thermal conductivity at ambient condition of various rocks becomes imperative to arrive at its threshold values.

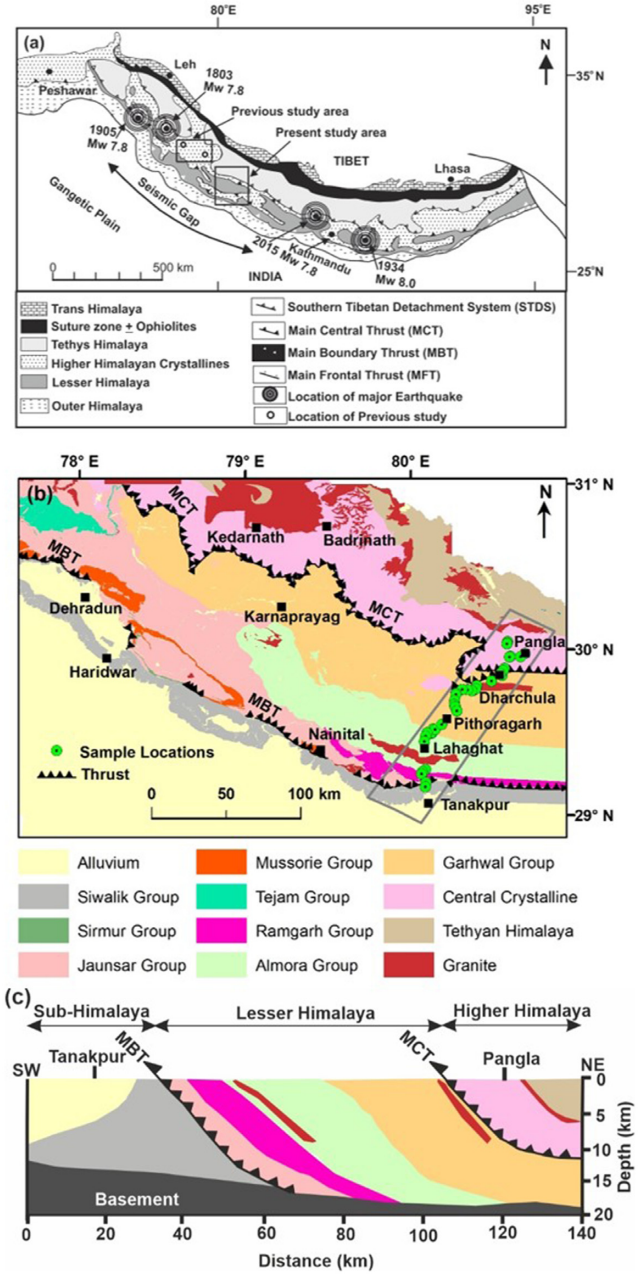

Figure 1. (a) Geological map of Himalaya (modified after Gansser 1964; Ray *et al.* 2007) showing the present study area and two locations of the previous study. (b) Geological map of Western Himalaya (source: Geological Survey of India, http://bhukosh.gsi.gov.in), showing sample locations of the present study. (c) Geological cross-section of the study region.

The present study area in the Western Himalaya (Fig. 1a) falls in the seismic gap, which is the segment of an active fault that has not experienced a significant magnitude earthquake for a long period. Here the seismic gap is about 700 km long and no major earthquakes have taken place since 1803. The current seismicity and geodetic measurements imply that this region is accumulating strain and a great earthquake is expected in the future (Bilham *et al.* 2001; Mahesh *et al.* 2013). West of this seismic gap one major earthquake occurred in 1905 (Kangra earthquake, M_w: 7.8), and in the east, two earthquakes occurred in 1934 (Nepal–Bihar earthquake; M_w: 8.0) and in 2015 (Nepal earthquake; M_w: 7.8). The earthquakes nucleate in the brittle zone. The depth of the brittle–ductile transition generally occurs in a narrow range of temperatures between 260 and 450 °C and may correspond to an isotherm in settings with consistent crustal lithologies and thermo-tectonic settings (Ranalli 1995). Thus, the temperature is an important parameter in rheological modelling. Therefore, thermal modelling for the seismic gap becomes essential to understand the earthquake mechanism and constrain brittle–ductile transition, and deep-seated rheology. To improve the accuracy of thermal modelling, the thermal conductivity of rocks plays a vital role; however, no thermal conductivity data currently exist on major rock formations for this region.

Table 1. Moho thickness and heat flow values surrounding the Himalayan Ranges.

Region	Moho thickness (km)	References	Heat flow (mW m^{-2})	References
		Himalayan Ranges		
Western Himalaya	28–53	Mandal *et al.* 2021	–	–
		Northeast region of Himalayan Ranges		
Tarim Basin	50	Wang *et al.* 2019	44–55	Wang 2001
Tian Shan	65	Shin *et al.* 2007	50–58	Wang 2001
The Junggar Basin	42–44	Gao *et al.* 2019	∼52	Wang 2001
The Altai Range	–	–	∼46	Wang 2001
Eastern Lhasa terrain	69–75	Gao *et al.* 2013	180–194	Tunnini *et al.* 2016
Qaidam basin	42	Wang *et al.* 2019	∼54	Wang 2001
Tibetan Plate	70–74	Li *et al.* 2006	∼84	Wang 2001
Sichuan Basin	36–40	Zhang *et al.* 2010	50–64	Wang 2001; Huang *et al.* 2012
		Southwest region of Himalayan Ranges		
Aravalli Province	38–50	Mandal *et al.* 2014	56–67	Roy & Rao 2000
Bundelkhand Craton	32–42	Jagadeesh & Rai 2008	32–41	Podugu *et al.* 2017
Damodar Basin	>40	Singh *et al.* 2015	69–79	Rao & Rao 1980
Singhbhum Thrust Zone	–	—	59–63	Rao & Rao 1974

Further, the Western Himalaya is accompanied by a large number of hot springs (GSI 1991), but except for the Puga Valley in Ladakh, Kashmir, no geothermal reservoir has been exploited yet. In spite of so much importance of the region, very limited thermal conductivity data from Western Himalaya has been reported to date. Available data include gneiss, metabasic and quartzite, from two boreholes drilled in the Loharinag-Pala and Tapovan-Vishnugarh areas located in Higher Himalayan crystalline of the Western Himalaya (Fig. 1a; Ray *et al.* 2007). These data even though are restricted to only two locations and a few lithologies but show significant variations within each lithology, which give more emphasis to the detailed study of the Western Himalaya. Also, no data are reported for heat flow, density and porosity from the whole Western Himalaya.

In fact, the published results on heat flow indicate that the whole Himalayan Ranges (Supporting Information Fig. S1) is almost devoid of heat flow values. The heat flow values reported till now are away from the Himalayan Ranges in different basins, sub-basins and shield areas of China, Tibet and India (Table 1). Data indicates that the heat flow in the regions that lie northeast of the Himalayan Ranges (covering basins and shield regions) show a wide range (44–194 mW m^{-2}), whereas the regions that lie southwest (basins and shield region) show a comparatively lower range (32–96 mW m^{-2}). Studies need to be done in the future to cover the heat flow of the Himalayan Ranges.

In this study, thermal and physical properties have been determined on samples that cover a comparatively larger area, cutting across Lesser and Higher Himalayan and consisting of sedimentary (sandstone, limestone and dolomitic limestone) as well as metamorphic (quartzite, slate, phyllite and schist) rocks, which form major lithologies of this region. Samples are collected in a 140-km long north–south profile from Tanakpur to Pangla (Fig. 1b) from fresh outcrops, the purpose of which is to fill a knowledge gap in thermal and physical properties of the major lithologic units from Western Himalaya. Present data sets, along with previous data, will be useful in detailed thermal and geodynamic modelling of the earthquake-sensitive region (Fig. 1a). To achieve this goal, we (i) measured thermal conductivity at water-saturated conditions using a steady-state method on 69 samples, (ii) determined the density and porosity of these rocks, (iii) characterized the mineralogy by petrography and geochemistry, (iv) correlated thermal conductivity variations for each variety of rocks with their composition and porosity and (v) compared the present result with the published data on the same suite of globally available sedimentary and metamorphic rock.

2 THE STUDY REGION

2.1 Geology of Himalaya

The Himalayan Mountains in Asia separate the plain of the Indian subcontinent from the Tibetan Plateau and are made up of uplifted sedimentary, metamorphic and intrusive igneous rocks. This is regarded as one of the world's youngest mountain ranges. The Himalaya orogenic Ranges formed as a result of horizontal compression of marine sediments caused by the northward drift-related collision of the Indian subcontinental with the Eurasian plate along the Indus-Tsangpo Suture Zone (ITSZ; Ali & Aitchison 2005; Gibbons *et al.* 2012). The collision caused the formation of several Late Cenozoic north dipping fault systems south of the ITSZ each with distinct litho-tectonic boundaries from north to south, such as the Southern Tibetan Detachment System (STDS), Main Central Thrust (MCT), Main Boundary Thrust (MBT) and Main Frontal Thrust (MFT; e.g. Valdiya 1980; Yin 2006). These thrust zones have divided the Himalayan orogeny into five slices from north to south; Trans Himalaya, Tethys Himalaya, Higher Himalaya, Lesser Himalaya and Outer Himalaya (Fig. 1a).

The Higher Himalaya is mainly composed of an approximately 10–30 km thick sequence of medium to high-grade metamorphic and metasedimentary rocks (various types of gneisses, schist, quartzite, marbles and amphibolites), which are frequently intruded by Ordovician

(∼500 Ma) and Lower Miocene (∼22 Ma) granites (Thakur 1987). The Higher Himalayan sequence is wide in the western part (especially in the Kashmir–Kishtwar region) and narrows down on the eastern side (Kumaun–Garhwal region). The Higher Himalaya, constituting the main metamorphic belt, overthrust the Lesser Himalaya formations along the MCT. It includes Precambrian crystallines of Paleoproterozoic to Cambrian in age overlain by a Phanerozoic sequence of the Tethys Himalaya. In the past, this region suffered maximum crustal shortening which is represented by the abnormally high uplift. Consequently, it exposed an 8–10 km thick slab of metamorphic and granitic rocks at the surface. In this zone, the maximum altitude is almost 5500 m.

In comparison, Lesser Himalaya is made up of marine sedimentary deposits (sandstone, limestone and dolomite), low to medium-grade metasedimentary rocks (quartzite, phyllite, schist, marble, slate and basic metavolcanics) with Ordovician granite intrusion. Sedimentary deposits comprise records of marine sediments of Proterozoic to Cambrian age and some sedimentary records of transgressing shallow sea during Permian, Upper Cretaceous and Middle Eocene—Lower Cenozoic period. The sedimentary sequences at most places are covered by thrust sheets of low and medium-grade crystalline rocks (metasedimentary and magmatic). These sequences are thrust over the Outer Himalaya along the MBT in the south and restricted from the Higher Himalaya by the MCT in the north. In this zone, which is about 13 to 16 km in width, with altitudes ranging between 1500 and 5000 m, inverted metamorphism can also be seen.

Based on the geographical location, the Himalayan range is divided into the Western Himalaya (Kashmir, Jammu, Himachal and Uttarakhand), Central Himalaya (Garhwal-Kumaon and Nepal) and Eastern Himalaya (Darjeeling, Sikkim, Bhutan and Arunachal Pradesh).

2.2 Geology of Western Himalaya

The Western Himalaya region (Fig. 1b) displays a complete cross-section of the five tectonic zones (Fig. 1c) described above. Samples of this study have been collected from two tectonic zones among them, that is Higher and Lesser Himalaya. The range extending southwards to the Himalayan foredeep is known as Gangetic Plains/Ganga basin (e.g. Valdiya 1980; Thakur 1993; Yin 2006). The region is mainly composed of sedimentary and metamorphic rocks (low to medium and medium to high-grade) with very few intrusions of igneous rocks. The rocks are Proterozoic to Eocene in age and are affected by many tectonic activities during the collision of the Indian and Eurasian plates.

2.3 Sample description

In a profile from Tanakpur to Pangla in the Western Himalaya covering the Higher and Lesser Himalaya 69 samples have been collected (Fig. 1b). Samples consist of sedimentary and metamorphic rocks, such as sandstone, limestone, dolomitic limestone, slate, phyllite, schist and quartzite. Cubical rock samples, with 10 to 12 cm on each side, have been collected from fresh outcrops/quarries along with the field description. Following care is taken while preparation of the disc samples. The discs are made considering the field descriptions. A portion of the rock sample is considered which are free from thin fractures, quartz veins and big crystals. Thus, rock samples are cored, cut and polished into cylindrical discs of 2.54 cm in diameter. The thickness of samples varies between 1.0 and 2.5 cm depending on rock type and grain size. Cut surfaces of disc samples are grounded and polished until the thickness variation is less than 0.01 mm. Petrography and geochemistry are done for the same part of the rock sample from where the disc is prepared.

3 MEASUREMENT METHODS

3.1 Thermal conductivity

A steady-state thermal conductivity meter (model QL-10^{TM}, Anter Corporation) has been used to measure the thermal conductivity of rock samples at ambient conditions. The disc sample is put into a stack and a constant temperature difference is maintained across the stack by keeping temperatures on the upper and lower side of the stacks at 45 and 5 °C, respectively, using the heater on the top and a water circulator in the bottom. To prevent heat loss to the surroundings, the stack is wrapped with thermal insulation material and the whole system is enclosed within an insulated housing. The contact resistance at the interfaces of the stack was minimized by applying a thermal compound (Thermal Joint Compound-Type 120 SILICONE) on the surfaces of the rock disc and subjecting the stack to a pressure of about 140 kPa. Measurements are taken after the sample has reached the steady-state condition. The thermal conductivity of the rock sample can be determined by measuring the voltage developed across the upper stack, the sample and the lower stack, respectively. The present setup takes about 30 minutes to attain a steady state. Before measuring the thermal conductivity, the instrument needs to be calibrated using reference specimens (Supporting Information Table S1 and Fig. S2).

The accuracy varies between ±3 to ±8 per cent depending on sample size and thermal conductivity. The precision of the measurement ranges from 0.01 to 0.03 for the thermal conductivity within the range of 1.5–3.0 $W\,m^{-1}\,K^{-1}$. Details about the apparatus, calibration and measurement procedure are given in Chopra *et al.* (2018, 2020).

3.2 Density and porosity

The density of the rock sample (ρ_{sample}) has been determined by the Archimedes principle, using the weight of the sample in the air (W_{air}), the weight of the sample in the water (W_{water}) and the density of water (ρ_{water}). The rock samples are weighed in the air and then in the water using a high precision balance (@Mettler-Toledo).

$$\rho_{sample} = \frac{W_{air} \times \rho_{water}}{W_{air} - W_{water}}. \quad (1)$$

Porosity (ϕ) of the rock is the volume of the open space in a rock (V_p) divided by the total volume of rock (V_r) (solid + space) then

$$\phi\,(\text{per cent}) = \frac{\text{Volume of voids } (V_p)}{\text{Total volume } (V_r)} \times 100. \quad (2)$$

In this study, cylindrical disc samples are dried in an oven for 12 hr and weights are measured (W_{dry}). Then, the rock samples are placed in desiccators for 10–15 min to remove the air from the pores and saturated with tap water under vacuum for at least 24 hr to allow water into the pores, and the weights of the water-saturated rock sample (W_{sat}) are measured. Porosity is calculated as,

$$\phi = \frac{W_{sat} - W_{dry}}{\pi \times R^2 \times H} \times 100, \quad (3)$$

where R and H are the radius and thickness of the sample, respectively.

3.3 Major oxides

After thin section screening, samples have been selected for geochemical analyses. The samples are crushed and converted into a fine powder using an agate mortar. The powder is finally sieved through a 200 ASTM mesh. Two grams of the finely powdered sample are filled in the collapsible aluminium cups with boric acid. These cups are then pressed under hydraulic pressure (at 25 Ton) to make the pellet. Major oxide concentrations have been determined by Wavelength-Dispersive X-ray Fluorescence Spectrometry (Model: PAN analytical-WDXRF) using pressed pellets. Details about the measurement method are given in Krishna *et al.* (2007).

4 CHARACTERIZATION OF THE SAMPLE

4.1 Petrography

The petrographic study has been carried out on sandstone, limestone, quartzite and schist. Photos of hand samples, typical photomicrographs and major-mineral of the studied rock types are shown in Fig. 2. Sandstones are dominantly composed of quartz, feldspar, mica and chlorite. The grains are subangular to subrounded. These are mature to submature (Fig. 2a). Limestones are mostly composed of calcite and dolomites with a small proportion of quartz, feldspar and mica (Fig. 2b). Quartzites are dominantly composed of quartz with a minor proportion of feldspar and muscovite. The quartz and mica grains are embedded within the silica matrix (Fig. 2c). Schists are composed of quartz, feldspar, mica, amphibole, chlorite and garnet as major constituents (Figs 2d and e). It is difficult to identify mineral grains of slate, and phyllite with the help of a petrographic microscope because of their fine-grained nature. These have been characterized based on hand specimens.

4.2 Geochemistry

The major oxide composition of the studied samples is given in Supporting Information Data set D1 and variations of major oxides with Al_2O_3 are shown in Fig. 3. Quartzites are characterized by a higher content of SiO_2 followed by sandstone, schist, phyllite, limestone and dolomitic limestone. SiO_2 variation in the studied samples can be related to the proportion of the quartz as well as the silica matrix. Al_2O_3 shows a negative correlation with SiO_2 and positive with other major oxides in sandstones and quartzites, except Fe_2O_3 for quartzites, whereas schist and phyllite are characterized with a positive correlation between Al_2O_3 and SiO_2. Most of the major oxides in schist show a negative correlation with Al_2O_3 except K_2O, while in phyllite MgO, CaO, Na_2O, TiO_2, P_2O_5 and MnO shows a negative correlation with Al_2O_3 and a positive correlation with Fe_2O_3 and K_2O. These plots show that the studied sandstone, quartzite, schist and phyllite are of quartz, clay and feldspar end member products, whereas the SiO_2 content in limestone is controlled by quartz but the negative correlation of CaO with SiO_2 (limestone $r = -0.92$, dolomitic limestone $r = -0.99$) suggests two different mineral phases in the studied limestone, namely SiO_2 from quartz and CaO from calcite. The negative correlation of Al_2O_3 with CaO and positive correlation with other major oxides in limestone indicate the presence of clay minerals. Dolomitic limestone, on the other hand, exhibits a negative correlation of Al_2O_3 with CaO, MgO and MnO and a positive correlation with Fe_2O_3, Na_2O, K_2O, TiO_2 and P_2O_5 indicating the presence of calcite, dolomite as well as feldspar and clay-bearing minerals present within the samples. Harker diagrams (Supporting Information Fig. S3) show wide variations in oxides within each rock type.

Further, the geochemical classification diagram (Fig. 4) indicates that the sandstones are arkose to subarkose and quartz arenite type, quartzites are characterized as arkosic to subarkosic, slate and phyllite are arkosic to lithic arenite, and schists are described as arkosic, lithic arenite to subarkose type. Thus, maximum compositional variation is observed in sandstone.

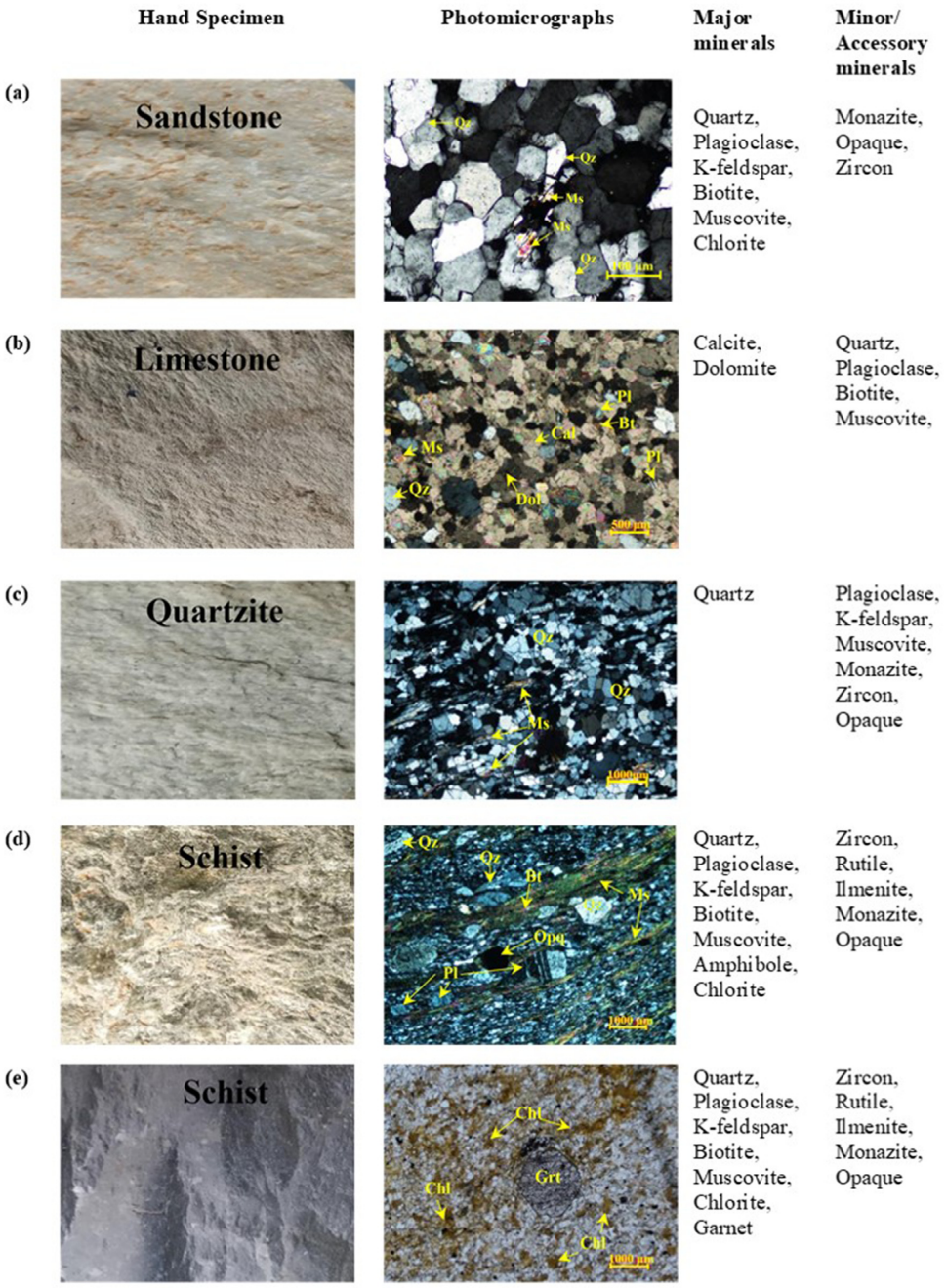

Figure 2. Hand specimen photographs, typical photomicrographs and overall major and minor minerals of the sedimentary and metamorphic rocks, Western Himalaya, India. Photomicrographs of (a) sandstone (in XPL: crossed polarized light), (b) siliceous limestone (in XPL), (c) quartzite (in XPL), (d) muscovite–biotite–schist (in XPL) and (e) garnet-bearing chlorite–schist (in PPL: plain polarized light). Chl: chlorite, Pl: plagioclase, Bt: biotite, Ms: muscovite, Cal: calcite, Dol: dolomite, Qz: quartz, Opq: opaque, Grt: garnet.

5 RESULTS

5.1 Thermal conductivity

Thermal conductivity for the studied rock samples at saturated conditions has been given in Supporting Information Data set D2. The variations of saturated thermal conductivity along with range, average and standard error are given in Table 2 and shown in Fig. 5.

Thermal conductivity is highest for quartzite (average: 5.4 $W\,m^{-1}\,K^{-1}$); moderate for sandstone, limestone and dolomitic limestone (average value ranges from 3.2 to 4.2 $W\,m^{-1}\,K^{1}$); and lowest for slate, phyllite and schist (average value ranges from 2.6 to 2.9 $W\,m^{-1}\,K^{-1}$). Thus, the thermal conductivity of the studied sedimentary rocks is higher than the metamorphic rocks except for quartzite. Standard errors of the thermal conductivity show higher values in limestone and dolomitic limestone than for phyllite, sandstone, quartzite and slate, while least

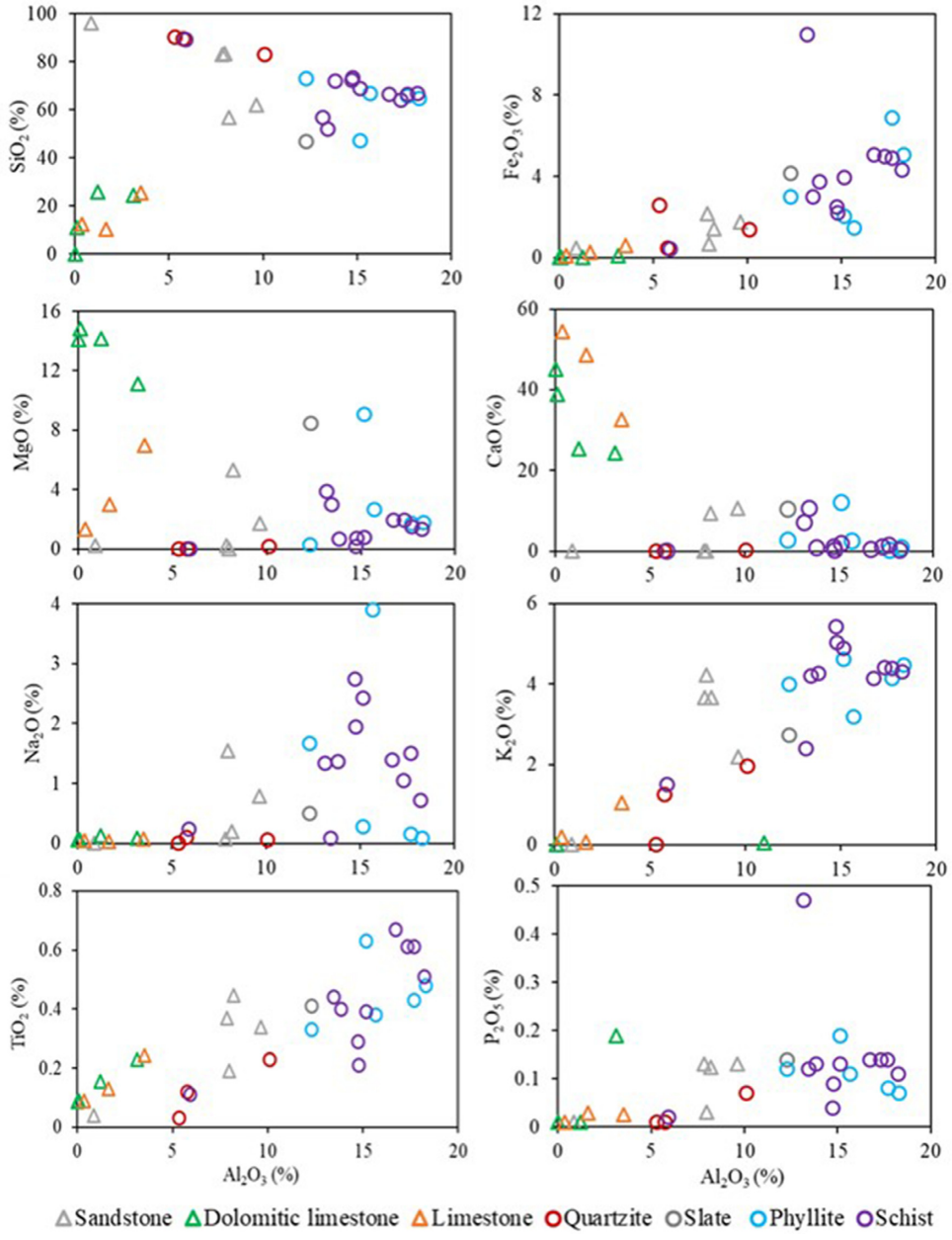

Figure 3. Bivariate plots show Al_2O_3 versus other major oxides for the sedimentary and the metamorphic rocks, Western Himalaya, India.

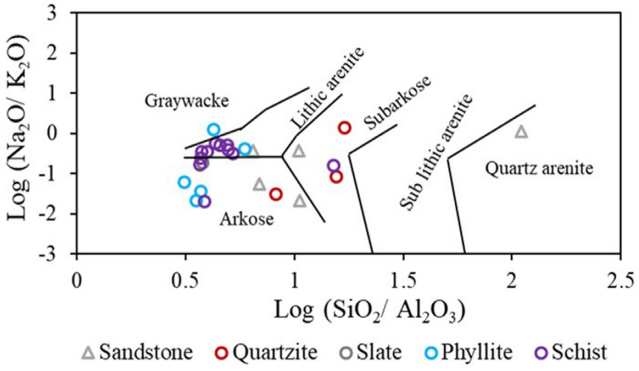

Figure 4. Geochemical classification diagram, based on the plot between log (Na_2O/K_2O) versus log (SiO_2/Al_2O_3) (Pettijohn *et al.* 1987) of the sedimentary and the metamorphic rocks, Western Himalaya, India.

Table 2. Thermal conductivity, density and porosity of the sedimentary and metamorphic rocks of the Western Himalaya, India.

Rock type	*N*	Thermal conductivity (W m^{-1} K^{-1})			Density (kg m^{-3})			Porosity (per cent)		
		Range	Avg.	S.E.	Range	Avg.	S.E.	Range	Avg.	S.E.
Sandstone	11	3.28–5.94	4.23	0.24	2529–2718	2590	15.2	0.3–1.6	1.0	0.1
Limestone	5	2.4–4.76	3.15	0.39	2566–2789	2690	37.0	0.3–1.0	0.8	0.1
Dolomitic limestone	8	3.35–6.12	3.58	0.36	2686–2847	2780	23.7	0.3–2.0	0.9	0.2
Quartzite	7	4.86–6.04	5.43	0.18	2552–2662	2630	15.1	0.4–1.5	0.7	0.2
Slate	5	2.33–3.29	2.94	0.16	2726–2750	2740	4.0	1.1–2.8	2.0	0.3
Phyllite	11	1.67–4.36	2.74	0.30	2545–2722	2650	17.4	0.4–2.7	1.2	0.2
Schist	22	1.93–4.23	2.57	0.11	2513–2776	2680	14.8	0.6–8.0	1.8	0.4

Note. N, number of samples; S.D., Standard deviation; Standard Error S.E.= S.D./sqrt(N.).

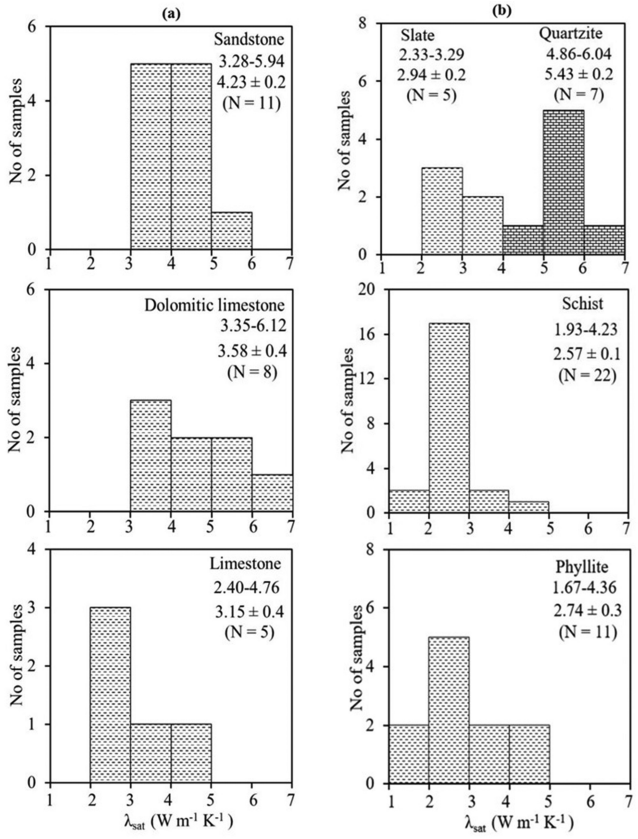

Figure 5. Histogram showing the distribution of saturated thermal conductivity (λ_{sat}) for the 69 studied samples. Columns (a) and (b) show sedimentary and metamorphic rocks, respectively. Values in each plot show range, mean, standard error and number of samples (*N*).

for schist (Table 2). But in general, for all the rock types, standard errors are low. Low standard errors indicate a comparatively homogeneous nature for each rock type. Anisotropy was also determined for a subset of samples and found to be very low (1.01 to 1.02).

5.2 Density

The density of the individual samples is given in Supporting Information Data set D2. Variations of density for each rock type (Fig. 6) and the average values with the standard error (Fig. 7) are given in Table 2. For the quartzite, sandstone and slate density varies in a small range compared to limestone, dolomitic limestone, schist and phyllite. The average density is slightly more for limestone, slate and dolomitic limestone (2690–2780 kg m^{-3}) than sandstone, quartzite, phyllite and schist (2590–2680 kg m^{-3}). Thus, it varies from 2590 to 2780 kg m^{-3} for the sedimentary rocks, whereas 2630 to 2740 kg m^{-3} for the metamorphic rocks.

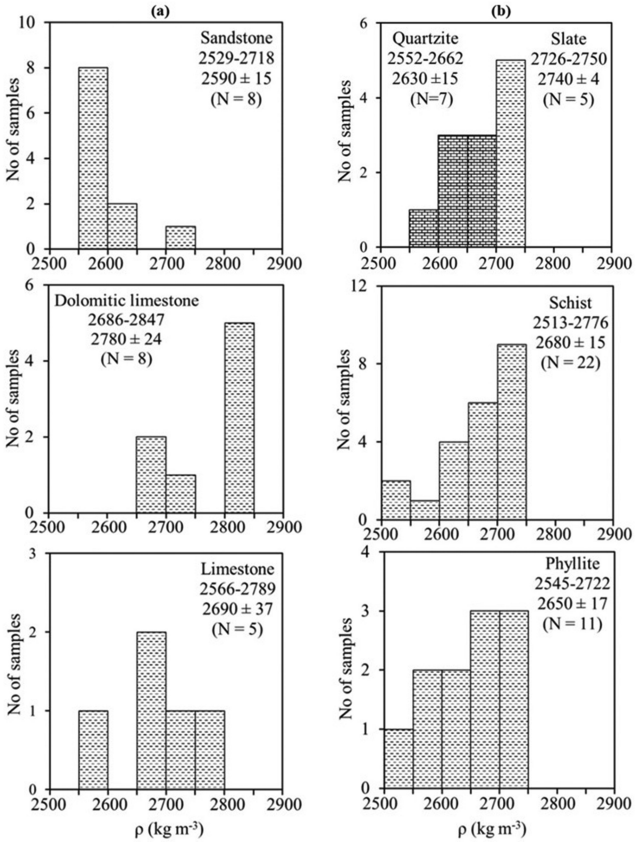

Figure 6. Histogram showing the distribution of density (ρ) for the 69 studied samples. Columns (a) and (b) show sedimentary and metamorphic rocks, respectively. Values in each plot show range, mean, standard error and number of samples (N).

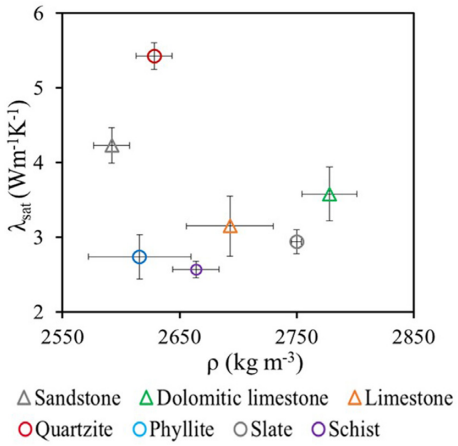

Figure 7. Bivariate plot shows saturated thermal conductivity (λ_{sat}) versus density (ρ) of the sedimentary and the metamorphic rocks, Western Himalaya, India.

5.3 Porosity

Porosity ranges from 0.3 to 2.8 per cent for individual samples, whereas it ranges from 0.7 to 2 per cent for different rock types. The average value is ∼2 per cent for slate and schist, and ∼1 per cent for the rest of the rocks (Table 2).

6 DISCUSSION

6.1 High thermal conductivity rocks of the Western Himalaya

The saturated thermal conductivity corresponds to *in situ* thermal conductivity and therefore it is considered while performing any modelling. The average saturated thermal conductivity of sedimentary rocks in the Western Himalaya is highest in sandstone and lowest in limestone, whereas in metamorphic rocks it is highest in quartzite and lowest in schist. Quartzite has the highest thermal conductivity among all rocks, whereas schist has the lowest (Fig. 7). The thermal conductivity of sedimentary rocks is higher than that of metamorphic rocks among the studied rocks, except for quartzite. The small thermal conductivity ranges within the slate and comparatively large ranges within other rock types (Fig. 8a) could be due to the differences in composition and their relative abundances from sample to sample. The thermal conductivity variations in sandstone, phyllite and schist can be correlated with most of the oxide data (SiO_2, Al_2O_3, Fe_2O_3, Na_2O, K_2O, TiO_2) except CaO, MgO, whereas for limestone and dolomitic limestone variations can be correlated with CaO, MgO. For the quartzite, the variations can be related to SiO_2, Al_2O_3, Fe_2O_3, K_2O and TiO_2 (Fig. 9). Further, analysis of geochemical data (Fig. 4) shows that the variations in thermal conductivity can be correlated well with the compositional change from arkose to quartz arenite type in sandstone, and arkose to subarkose type in quartzite. It is lowest for arkose type, and highest for quartz arenite type.

The observed variations in geochemical composition are due to the relative abundances in mineralogy within a particular rock type, and thus they control thermal conductivity, as various minerals depict different thermal conductivity. Among the rock-forming minerals observed in the studied samples (Table 3), quartz has the highest thermal conductivity (avg.: 7.6 $Wm^{-1}K^{-1}$), whereas chlorite, dolomite, calcite, rutile, zircon and garnet have intermediate values (avg.: 3.6–5.5 $Wm^{-1}K^{-1}$) and feldspar, biotite, muscovite and ilmenite have comparatively lower values (avg.: 1.8–2.5 $Wm^{-1}K^{-1}$). Within each rock type large variations in thermal conductivity have been observed in the study (Fig. 8a, Table 2), as well as in previous studies from different tectonic/geological provinces of the world (Fig. 10a, Supporting Information Table S2). The systematic variations in thermal conductivity within a rock type for the difference in mineralogy have been noticed in sandstone, quartzite, phyllite, mica schist and schist. Feldspathic, non-feldspathic and quarzitic sandstone collected from different tectonic regions show variation in thermal conductivity (Zierfuss & Van der Vliet 1956). In the Witwatersrand Basin, South Africa, the variation in thermal conductivity have been observed between non-feldspathic, feldspathic and chlorite bearing quartzite (Bullard 1939). Similarly, in the Singhbhum Thrust Zone, India the feldspathic, chlorite and biotite schist shows large variations in thermal conductivity (Verma *et al.* 1966). The phyllite and mica schist, rich in graphite, chlorite, quartz, etc., show variations in thermal conductivity (Gegenhuber & Kienler 2017). Thus, the relative abundances of minerals and the wide range in thermal conductivity of the minerals controlled the thermal conductivity and its variations within a rock type.

Further, there are variations in average thermal conductivity from one rock to the other rock type (Fig. 7). The dominance of quartz in quartzite shows higher thermal conductivity, and the decrease in thermal conductivity from sandstone, dolomitic limestone, limestone, slate and phyllite to schist is related to the presence of feldspar, biotite, garnet and/or clay minerals (Fig. 2), which lowers the thermal conductivity values. Dolomitic limestone has higher thermal conductivity than limestone due to the higher thermal conductivity of dominant mineral dolomite.

Thermal conductivity for a particular rock type also decreases with increasing porosity, although the trend could be different for different rocks (Jõeleht & Kukkonen 2002; Jõeleht *et al.* 2002; Popov *et al.* 2003). In the present study, porosity is very low and the correlation between thermal conductivity and porosity for each rock type shows different characteristics. Limestone, dolomitic limestone and sandstone show a decreasing trend in thermal conductivity with increasing porosity for most of the samples. But for other rocks, no correlation is observed (Fig. 11a). But as the porosity of the rocks is very low, the variation in thermal conductivity of the studied rocks depends more on the variation in mineralogical composition and little on porosity. The low porosity also reflected in matrix thermal conductivity values (Supporting Information Data set D2).

Considering average thermal conductivity values reported in previous studies, sandstone of the Western Himalaya falls on the higher side, whereas limestone, quartzite falls in the middle, and slate, phyllite, schist fall on the lower side of the observed wide range (Fig. 10a).

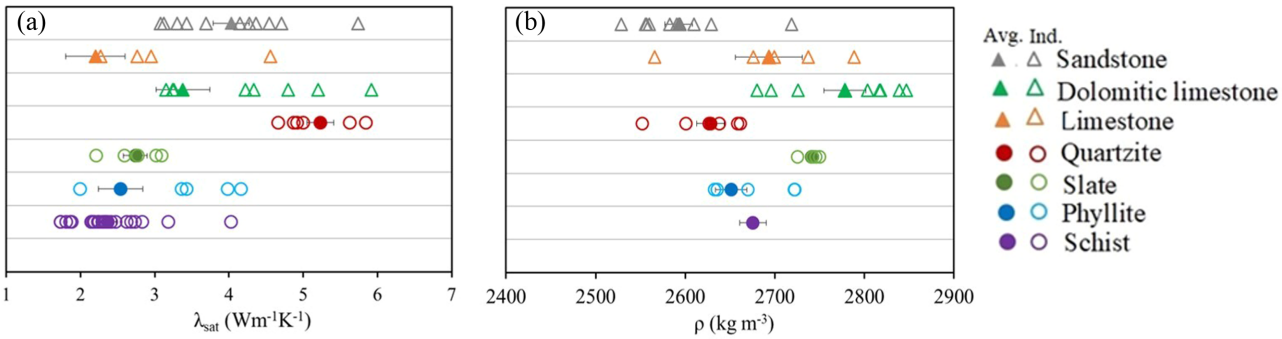

Figure 8. (a) Thermal conductivity and (b) density of the sedimentary and metamorphic rocks of the Western Himalaya, India. Ind: individual values; Avg.: average values. Standard errors are shown with average values by solid grey lines.

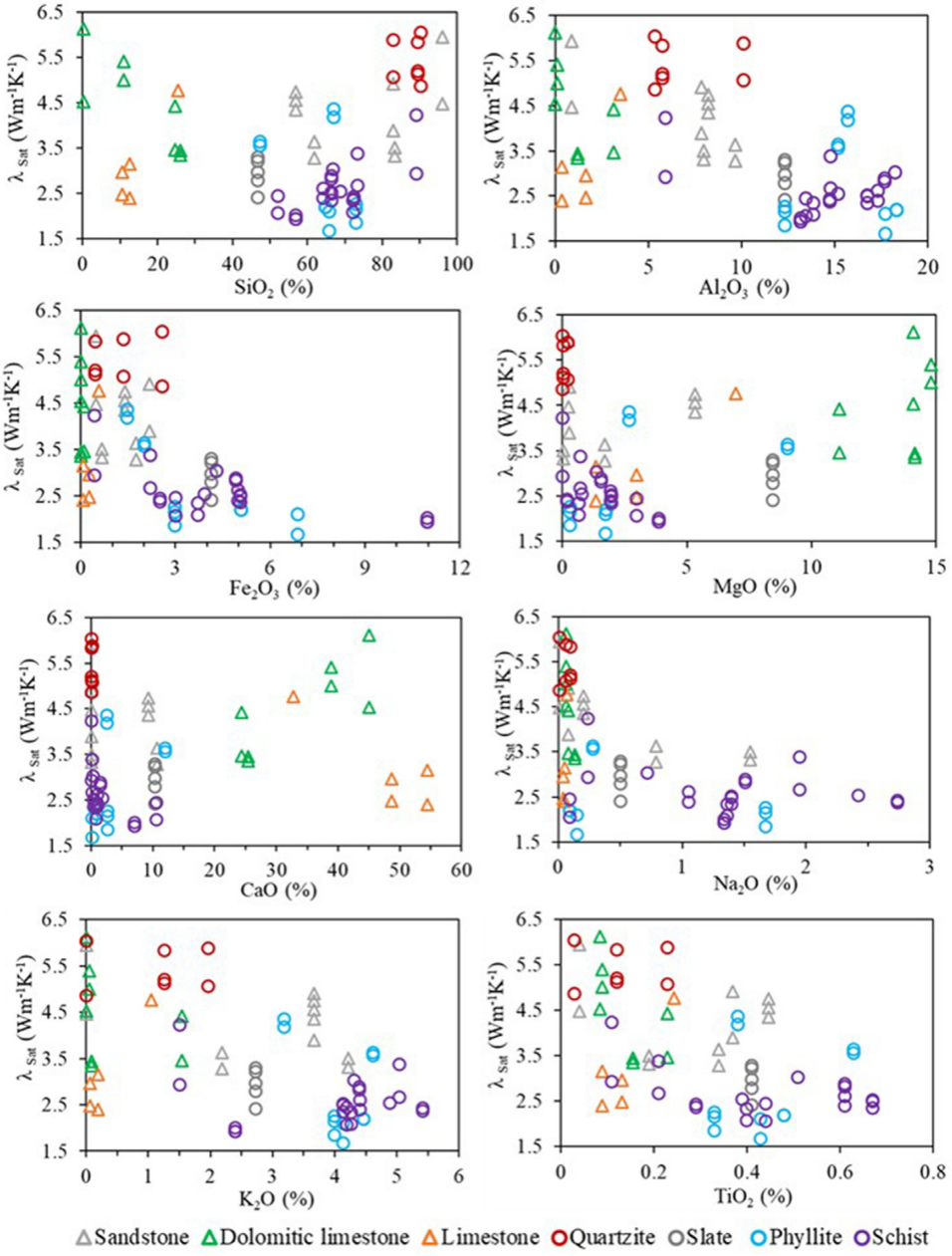

Figure 9. Bivariate plots showing saturated thermal conductivity (λ_{sat}) versus major oxides of the sedimentary and the metamorphic rocks, Western Himalaya, India.

However, the average thermal conductivity value of quartzite in this study, is almost the same as the previously reported value from the other part of the Western Himalaya (Ray *et al.* 2006), which gives more confidence about the thermal conductivity values of the quartzite from the Western Himalaya.

6.2 High density and low porosity rocks of the Western Himalaya

The sedimentary rocks in the Western Himalaya have higher density (Fig. 10b) and lower porosity, than the sedimentary rocks in general. Also, these rocks have similar density and porosity ranges as that of the metamorphic rocks for the same region (Fig. 11, Table 2). Average density values in the investigated rocks fall on the higher side of the large range reported in the literature for the sedimentary rocks, whereas the lower side for the metamorphic rocks (Fig. 10b, Supporting Information Table S3). The high-dense and low-porous sedimentary rocks could have been formed by the tectonic and post-tectonic activity in this region, which is activated from Cambrian and make them compact. In this process, rocks may have undergone low-metamorphism at a certain depth and came to the surface at present by exhumation. The petrographic study reveals that the muscovite grains in sandstone are aligned in one direction, which can be attributed to the early stage of metamorphism (for example, Fig. 2a). The compactness of the rocks corroborates the low porosity, and thus the observed density will be the

Table 3. Thermal conductivity of minerals those are observed in the studied samples.

Sl no.	Mineral	Thermal conductivity (W m^{-1} K^{-1})		References
		Range	Avg.	
1	Quartz	6.5–11.3	7.64	4, 9, 6
2	Plagioclase	1.47–2.35	1.79	4
3	K-feldspar	2.26–2.43	2.33	1, 2, 4
4	Biotite	1.70–2.34	2.03	2, 4, 5, 7, 8
5	Chlorite	4.35–6.18	5.17	2, 3, 5
6	Muscovite	2.0–2.88	2.36	2, 4, 7, 8
7	Dolomite	–	5.51	4
8	Calcite	–	3.59	4
9	Rutile	4.89–5.12	5.01	2, 4, 8
10	Zircon	–	4.54	2, 4
11	Ilmenite	2.2–2.92	2.51	2, 4, 5, 8
12	Garnet	3.09–5.65	4.2	4

References. 1, Sass (1965); 2, Horai & Simmons (1969); 3, Clarke (1969); 4, Horai (1971); 5, Horai & Baldridge (1972); 6, Beck *et al.* (1978); 7, Dortman (1984), 8, Popov *et al.* (1987); 9, Joeleht & Kukkonen (2002).

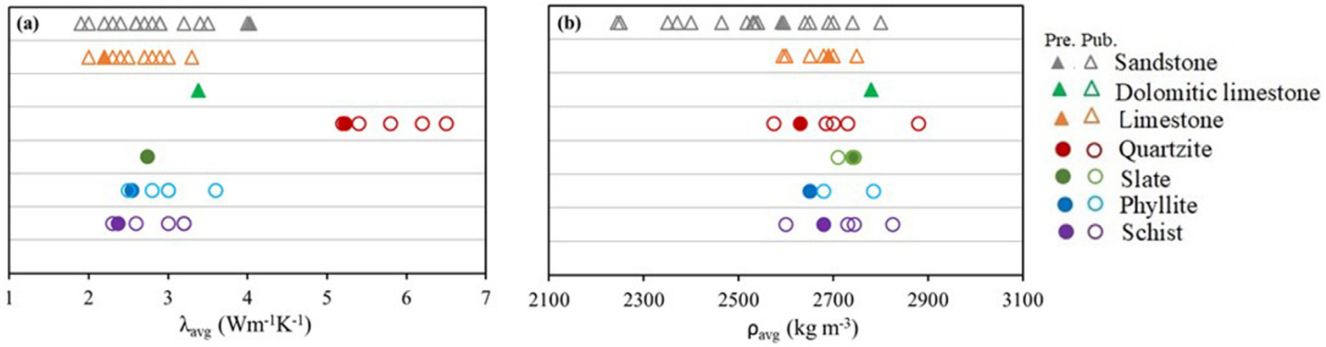

Figure 10. (a) Average thermal conductivity and (b) average density of sedimentary and metamorphic rocks. Pre: the present data from the Western Himalaya, India; Pub: the published data from the various regions of the world. For details, see Supporting Information Tables S2 and S3.

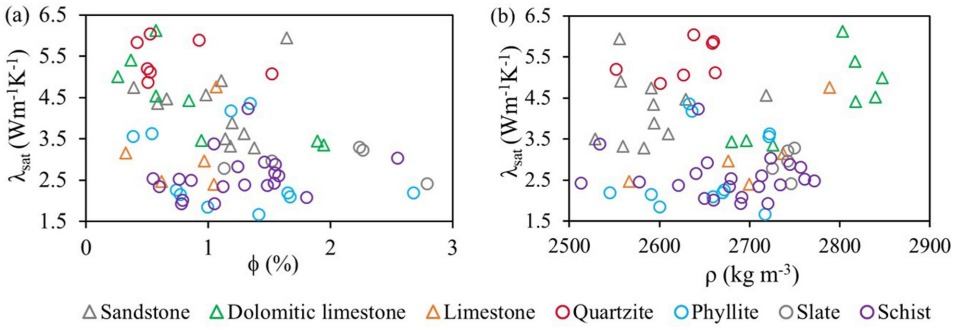

Figure 11. Bivariate plot shows saturated thermal conductivity (λ_{sat}) versus (a) porosity ϕ; (b) density ρ.

same as the matrix density of the rocks. Except for slate, the density of each rock type varies in a relatively wide range (Fig 8b, Table 2). In the sedimentary rock, density is higher for the limestone and dolomitic limestone compared to the sandstone, whereas in the metamorphic rock, it is higher for slate compared to schist, quartzite and phyllite. Variations in density within a specific rock type can be correlated with compositional changes reflected in the variation of the oxide data within them (Supporting Information Fig. S4).

Density shows a positive correlation with thermal conductivity for a few rock types (Fig. 11b), but the correlation varies from one rock to another, indicating that changes in density and thermal conductivity are different for different rocks. A positive correlation is noted between density and thermal conductivity for sandstone, limestone and dolostone in the Tarim Basin and Lino Viluy oil and gas-bearing province (Semenov *et al.* 2018; Li *et al.* 2019). On the other hand, a negative correlation is observed in igneous rocks, especially in granitoids (Kukkonen & Peltoniemi 1998; Chopra *et al.* 2018, 2020). The anomalous density and porosity of the Himalayan rocks will provide new inputs for the geodynamical modelling of the region.

7 CONCLUSIONS

This is the first systematic study of thermal and physical parameters for the Western Himalaya's sedimentary and metamorphic rocks, revealing comparatively high thermal conductivity, high density and low porosity, in comparison to the similar rock types available elsewhere. As a result, the reported thermal and physical properties, as well as geochemical and petrological data from the rocks in the Western Himalayan seismic gap, will be a useful database for thermal and geodynamic modelling of this region. Additionally, these properties will also be useful for geothermal exploration, as in the Western Himalaya many hot springs are present all along with the Himalayan Ranges and Puga Valley is already a potential for geothermal exploration. Significant outcomes are from the present study as follow:

(i) The thermal conductivity of the studied metamorphic rocks is generally lower than the sedimentary rocks, except for quartzite. Thermal conductivity is highest for quartzite (5.4 ± 0.2 W m^{-1} K^{-1}), intermediate for sandstone (4.2 ± 0.2 W m^{-1} K^{-1}), dolomitic limestone (3.6 ± 0.4 W m^{-1} K^{-1}) and limestone (3.2 ± 0.4 W m^{-1} K^{-1}) and lowest for slate (2.9 ± 0.2 W m^{-1} K^{-1}), phyllite (2.7 ± 0.3 W m^{-1} K^{-1}) and schist (2.6 ± 0.1 W m^{-1} K^{-1}).

(ii) For sandstone and quartzite, the variation in thermal conductivity can be correlated well with variation in composition from arkose to quartz arenite, which is lowest for arkose and highest for quartz arenite type. Also, in other rock types, variation can be correlated more with compositional change and very little with porosity.

(iii) The density of both the rock types, sedimentary and metamorphic, have similar values and vary in a wide range (2590 to 2780 kg m^{-3} and 2630 to 2740 kg m^{-3}, respectively). Highly dense and low porous ($<$2 per cent) sedimentary rock could be due to the tectonic/post-tectonic activity of the region, which makes these rocks compact or could be due to low metamorphism at a certain depth which exhumed and came to the surface at present.

(iv) The study deals with thermal conductivity measurement of rocks along with comprehensive compositional descriptions, which is missing in most of the earlier studies, and therefore will be helpful to produce better predictive models of thermal conductivity.

ACKNOWLEDGMENTS

The research presented here is supported by the Council of Scientific & Industrial Research grants [SHIVA (MLP-0001–28-FBR-1) and PROBHIM (MLP-FBR-0003)]. We acknowledge K. Mahesh for the preparation of samples required for laboratory analysis, A. Keshav Krishna for the analysis of major oxides in the XRF laboratory of CSIR-NGRI, and O. P. Pandey and Nishu Chopra for useful suggestions. Our sincere thanks to the reviewers, Ilmo Kukkonen and Derrick Hasterok, editor J. C. Afonso and assistant editor Louise Alexander, for their critical as well as constructive comments and valuable suggestions that helped to improve the paper substantially. We thank the Director, CSIR-National Geophysical Research Institute (NGRI), Hyderabad, for his continuous support. The reference number of the paper is NGRI/Lib/2020/Pub-50. All data used here are available in the supporting information.

DATA AVAILABILITY

The data underlying this paper are available in the paper and its online supplementary material.

REFERENCES

Ali, J.R. & Aitchison, J.C., 2005. Greater India, *Earth Sci. Rev.*, **72,** 169–188.

Balkan, E., Erkan, K. & Şalk, M., 2017. Thermal conductivity of major rock types in western and central Anatolia regions, Turkey, *J. Geophys. Eng.,* **14,** 909–919.

Beck, A.E., Darbha, D.M. & Schloessin, H.H., 1978. Lattice conductivities of single-crystal and polycrystalline materials at mantle pressures and temperatures, *Phys. Earth planet. Inter.,* **17,** 35–53.

Bilham, R., Gaur, V.K. & Molnar, P., 2001. Himalayan Seismic Hazard, *Science,* **293,** 1442–1444.

Birch, F. & Clark, H., 1940. The thermal conductivity of rocks and its dependence upon temperature and composition, *Am. J. Sci.,* **238,** 613–635.

Birch, F., 1950. Flow of Heat in the front range, Colorado, *Bull. geol. Soc. Am.,* **61,** 567–630.

Bullard, E.C., 1939. Heat flow in South Africa, *Proc. R. Soc. A,* **173,** 474–502.

Cermak, V. & Rybach, L., 1982. Thermal properties: thermal conductivity and specific heat of minerals and rocks, in *Numerical Data and Functional Relationships in Science and Technology, New Series, Physical Properties of Rocks,* pp. 305–343, ed. Angenheister, G., Springer.

Chopra, N., Ray, L., Satyanarayanan, M. & Elangovan, R., 2018. Evaluate best-mixing model for estimating thermal conductivity for granitoids from mineralogy: a case study for the granitoids of the Bundelkhand craton, central India, *Geothermics,* **75,** 1–14.

Chopra, N., Ray, L., Dey., S. & Mitra, A., 2020. Thermal conductivity, density, petrological and geochemical characteristics of granitoids from Singhbhum craton, eastern India, *Geothermics,* **87,** 101855.

Clarke, S.M., 1969. A manual of the physical constants of rocks (Russian Translation). *Mir, Moscow,* 542.

Clauser, C., 2006. Geothermal energy. Landolt-Börnstein, Group VIII, *Adv. Mater. Technol.,* **3,** 493–604.

Dortman, N.B., 1984. Physical Properties of Rocks and Mineral Resources (Petrophysics): *a Manual of Geophysics. Nedra, Moscow,* 455.

Feng, J., Gao, Z., Zhu, R., Luo, Z. & Zhang, L., 2013. The application of thermal conductivity measurements to the Kuqa River profile, China, and implications for petrochemical generation. *Springer Plus,* **2,** 1–6.

Forster, H.J., Forster, A., Oberhansli, R. & Stromeyer, D., 2010. Lithospheric composition and thermal structure of the Arabian Shield in Jordan, *Tectonophysics,* **481,** 29–37.

Fuchs, S., Schütz, F., Forster, H. J. & Forster, A., 2013. Evaluation of common mixing models for calculating bulk thermal conductivity of sedimentary rocks: correction charts and new conversion equations, *Geothermics,* **47,** 40–52.

Gansser, A., 1964. *The Geology of the Himalayas,* Wiley, pp. 289.

Gao, R., Chen, C., Lu, Z., Brown, L.D., Xiong, X., Li, W. & Deng, G., 2013. New constraints on crustal structure and Moho topography in

Central Tibet revealed by SinoProbe deep seismic reflection profiling, *Tectonophysics,* **606,** 160–170.
Gao, G., Hou, J., Kang, G., Bai, C., Wen, L., Zhao, H. & Shi, L., 2019. Crustal thickness and lithospheric thermal state beneath the Junggar Basin and adjacent mountain ranges, Northwest China, *J. Asian Earth Sci.,* **184,** 103802.
Gegenhuber, N. & Kienler, M., 2017. Improved petrographic-coded model and its evaluation to determine a thermal conductivity log, *Acta Geophys*., **65,** 103–118.
Gibbons, A., Barckhausen, U., Van den Bogaard, P., Hoernle, K., Werner, R., Whittaker, J. & Müller, 2012. Constraining the Jurassic extent of greater India: tectonic evolution of the west Australian margin, *Geochem Geophys*., 13**.**
Goy, L., Fabre, D. & Menard, G., 1996. Modelling of rock temperatures for deep alpine tunnel projects, *Rock Mech .Rock Eng.*, **29,** 1–18.
GSI, 1991. Geothermal Atlas of India, Special Publication.19, *Geol. Sur. India.*
Horai, K.-I., 1971. Thermal conductivity of rock-forming minerals, *J. geophys. Res.,* **76,** 1278–1308.
Horai, K.-I. & Baldridge, S., 1972. Thermal conductivity of nineteen igneous rocks, II estimation the thermal conductivity of rock from the mineral and chemical compositions, *Phys. Earth planet. Inter.,* **5,** 157–166.
Horai, K.-I. & Simmons, G., 1969. Thermal conductivity of rock-forming minerals, *Earth planet. Sci. Lett.,* **6,** 359–368.
Huang, F., Liu, Q.Y. & He, L.J., 2012. Tectono-thermal modeling of the Sichuan Basin since the Late Himalayan period, *Chin. J. Geophys.,* **55,** 3742–3753.
Jagadeesh, S. & Rai, S.S., 2008. Thickness, composition, and evolution of the Indian Precambrian crust inferred from broadband seismological measurements, *Precambrian Res.,* **162,** 4–15.
Jõeleht, A. & Kukkonen, I.T., 2002. Physical properties of Vendian to Devonian sedimentary rocks in Estonia. *GFF,* **124,** 65–72.
Jõeleht, A., Kirsimäe, K, Shogenova, A., Šliaupa, S., Kukkonen, I.T., Rastenie, V. & Zabele, A., 2002. Thermal conductivity of Cambrian siliciclastic rocks from the Baltic Basin, *Proc. Estonian Acad. Sci. Geol.,* **51,** 5–15.
Kappelmeyer, O. & Haenel, R., 1974. Geothermics with special reference to application, *Berlin Gebrueder Borntraeger Geoexploration Monographs Series,* **4**.
Kukkonen, I.T. & Peltoniemi, S., 1998. Relationships between thermal and other petrophysical properties of rocks in Finland, *Phys. Chem. Earth,* **23,** 341–349.
Kukkonen, I.T., Jokinen, J. & Seipold, U., 1999. Temperature and pressure dependencies of thermal transport properties of rocks: implications for uncertainties in thermal lithosphere models and new laboratory measurements of high-grade rocks in the central Fennoscandian shield, *Surv. Geophys.,* **20,** 33–59.
Krishna, A.K., Murthy, N.N. & Govil, P.K., 2007. Multi-element analysis of soils by wavelength dispersive X-ray fluorescence spectrometry, *At. Spectrosc.,* **28,** 202–214.
Lawless, J.V., Ward, M. & Beardsmore, G., 2010. The Australian code for geothermal reserves and resources reporting: practical experience, in *Proceedings of the World Geothermal Congress*.
Li, X., Liu, S. & Feng, C., 2019. Thermal properties of sedimentary rocks in the Tarim Basin, northwest China, *AAPG Bull.,* **103,** 1605–1624.
Lichtenecker, K., 1926. Die dielektriziteatskonstante naturalicher und kunstlicher mischkorper. *Phy. Z.,* **27,** 115–158.
Mahesh, P., Rai, S.S., Sivaram, K., Paul, A., Gupta, S., Sarma, P.R. & Gaur, V.K., 2013. One dimensional reference velocity model and precise locations of earthquake hypocenters in the Kumaon- Garhwal Himalaya, *Bull. seism. Soc. Am.,* **103,** 328–339.
Mandal, B., Sen, M.K., Vaidya, V.R. & Mann, J., 2014. Deep seismic image enhancement with the common reflection surface (CRS) stack method: evidence from the Aravalli–Delhi fold belt of northwestern India, *Geophys. J. Int.,* **196,** 902–917.
Mandal, P., Srinivas, D., Suresh, G. & Srinagesh, D., 2021. Modelling of crustal composition and Moho depths and their Implications toward seismogenesis in the Kumaon–Garhwal Himalaya, *Sci. Rep.,* **11,** 1–13.
Mareschal, J.C., Poirier, A., Rolandone, F., Bienfait, G., Gariépy, C., Lapointe, R. & Jaupart, C., 2000. Low mantle heat flow at the edge of the North American continent, Voisey Bay, Labrador, *Geophys. Res. Lett.,* **27,** 823–826.
Pettijohn, F. J., Potter, P. E. & Siever, R., 1987. *Sand and Sandstone,* Springer, pp. 553.
Pigford, T., 1982. Geological disposal of radioactive waste, *Chem. Eng. Prog.,* **78,** 18–26.
Podugu, N., Ray, L., Singh, S.P. & Roy, S., 2017. Heat flow, heat production, and crustal temperatures in the Archaean Bundelkhand craton, north-central India: implications for thermal regime beneath the Indian shield, *J. geophys. Res.,* **122,** 5766–5788.
Popov, Y., Berezin, V., Soloviov, G., Romuschkevitch, R., Korosteliov, V., Kostiurin, A. & Kulikov, A., 1987. Thermal conductivity of minerals, *Izv. Phys. Solid Earth,* **23,** 245–253.
Popov, Y., Tertychnyi, V., Romushkevich, R., Korobkov, D. & Pohl, J., 2003. Interrelations between thermal conductivity and other physical properties of rocks: experimental data, *Pure appl. Geophys.,* **160,** 1137–1161.
Ranalli, G., 1995. *Rheology of the Earth,* Springer Science & Business Media.
Rao, G.V. & Rao, R.U.M., 1980. A geothermal study of the Jharia Gondwana Basin (India): heat flow results from several holes and heat production of basement rocks, *Earth planet. Sci. Lett.,* **48,** 397–405.
Rao, R.U.M. & Rao, G.V., 1974. Results of some geothermal studies in Singhbhum thrust belt, India, *Geothermics,* **3,** 153–161.
Roy, R.F., Beck, A.E. & Touloukian, Y.S., 1981. Thermophysical properties of rocks, in *Physical Properties of Rocks and Minerals,* McGraw-Hill CINDAS Data Series on Material Properties, Vol. 11–12, pp. 409–502, eds Touloukian, Y.S., Judd, W.R. & Roy, R.F..
Roy, S. & Rao, R.U.M., 2000. Heat flow in the Indian shield, *J. geophys. Res.,* **105,** 25 587–25 604.
Roy, S., Ray, L., Bhattacharya, A. & Srinivasan, R., 2008. Heat flow and crustal thermal structure in the Late Archaean Closepet Granite batholith, south India, *Int. J. Earth Sci.,* **97,** 245–256.
Ray, L., Kumar, P. S., Reddy, G.K., Roy, S., Rao, G.V., Srinivasan, R. & Rao, R.U.M., 2003. High mantle heat flow in a Precambrian granulite province: evidence from southern India, *J. geophys. Res.,* **108,** 2084.
Ray, L., Förster, H.J., Schilling, F.R. & Förster, A., 2006. Thermal diffusivity of felsic to mafic granulites at elevated temperatures, *Earth planet. Sci. Lett.,* **251,** 241–253.
Ray, L., Bhattacharya, A. & Roy, S., 2007. Thermal conductivity of Higher Himalayan crystallines from Garhwal Himalaya, India, *Tectonophysics,* **434,** 71–79.
Ray, L., Chopra, N., Hiloidari, S., Naidu, N.N. & Kumar, V., 2021. Thermal conductivity of granitoids of varying composition up to 300° C and implications for crustal thermal models, *Geophys. J. Int.,* **227,** 316–332.
Rutqvist, J., Barr, D., Birkholzer, J. T., Chijimatsu, M., Kolditz, O., Liu, Q. & Zhang, C., 2008. Results from an international simulation study on coupled thermal, hydrological, and mechanical processes near geological nuclear waste repositories, *Nucl. Technol.,* **163,** 101–109.
Rybach, L. & Pfister, M., 1994. Temperature predictions and predictive temperatures in deep tunnels, *Rock Mech. Rock Eng.,* **27,** 77–88.
Rybach, L., Wilhelm, J. & Gorhan, H., 2003. Geothermal use of tunnel waters—a Swiss specialty, in *International Geothermal Conference,* Reykjavík, pp. 17–23.
Sass, J.H., 1965. The thermal conductivity of fifteen feldspar specimens, *J. geophys. Res.,* **70,** 4064–4065.
Semenov, V.P., Zheleznyak, M.N., Kirillin, A.R. & Zhizhin, V.I., 2018. Thermal conductivity of the sedimentary rocks in the Leno Viluy oil- and gas-bearing province, *Earth's Cryosphere,* **XXII,** 26–34.
Shen, Y.J., Wang, Y.Z., Zhao, X.D., Yang, G.S., Jia, H.L. & Rong, T.L., 2018. The influence of temperature and moisture content on sandstone thermal conductivity from a case using the artificial ground freezing (AGF) method, *Cold Reg. Sci. Technol.,* **155,** 149–160.
Shin, Y.H., Xu, H., Braitenberg, C., Fang, J. & Wang, Y., 2007. Moho undulations beneath Tibet from GRACE-integrated gravity data, *Geophys. J. Int.,* **170,** 971–985.

Singh, A.P., Kumar, N. & Zeyen, H., 2015. Three-dimensional lithospheric mapping of the eastern Indian shield: a multi-parametric inversion approach, *Tectonophysics,* **665,** 164–176.
SKB, 2005. Preliminary safety evaluation for the Simpevarp subarea. Based on data and site descriptions after the initial site investigation stage. Tech. Rep., TR–05-12.
Thakur, V. C., 1987. Plate tectonic interpretation of the Western Himalaya, *Tectonophysics,* **134,** 91–102.
Thakur, V.C., 1993. *Geology of Western Himalaya,* Pergamon Press, pp. 366.
Tunini, L., Jiménez-Munt, I., Fernandez, M., Vergés, J., Villaseñor, A., Melchiorre, M. & Afonso, J.C., 2016. Geophysical-petrological model of the crust and upper mantle in the India-Eurasia collision zone, *Tectonics,* **35,** 1642–1669.
Valdiya, K.S., 1980. *Geology of the Kumaon Lesser Himalaya,* Wadia Institute of Himalaya, pp. 291.
Verma, R.K., Rao, R.U.M. & Gupta, M.L., 1966. Terrestrial heat flow in Mosabani mine, Singhbhum district, Bihar, India, *J. geophys. Res.,* **71,** 4943–4948.
Wang, J., Xu, C., Luo, Z., Wu, Y., Zhou, B. & Yan, J., 2019. An approach to moho topography recovery using the on-orbit GOCE gravity gradients and its applications in Tibet, *Remote Sens.,* **11,** 1567.
Wang, Y., 2001. Heat flow pattern and lateral variations of lithosphere strength in China mainland: constraints on active deformation, *Phys. Earth planet. Inter.,* **126,** 121–146.
Woodside, W. & Messmer, J.H., 1961a. Thermal conductivity of porous media. I. Unconsolidated sands, *J. Appl. Phys.,* **32,** 1688–1699.
Woodside, W. & Messmer, J.H., 1961b. Thermal conductivity of porous media. 2. Consolidated rocks, *J. Appl. Phys.,* **32,** 1699–1706.
Yin, A., 2006. Cenozoic tectonic evolution of the Himalayan orogen as constrained by along-strike variation of structural geometry, exhumation history, and foreland sedimentation, *Earth Sci. Rev.*, **76,** 1–131.
Zhang, Z., Yuan, X., Chen, Y., Tian, X., Kind, R., Li, X. & Teng, J., 2010. Seismic signature of the collision between the east Tibetan escape flow and the Sichuan Basin, *Earth planet. Sci. Lett.,* **292,** 254–264.
Zoth, G. & Haenel, R., 1988. Thermal conductivity, in *Handbook of Terrestrial Heat-Flow Density Determination,* pp. 449–468, eds Haenel, R., Rybach, L. & Stegena, L., Kluwer.
Zierfuss, H. & Van der Vliet, G., 1956. Laboratory measurements of heat conductivity of sedimentary rocks, *AAPG Bull.,* **40,** 2475–2488.
Li, S., Mooney, W.D. & Fan, J., 2006. Crustal structure of mainland China from deep seismic sounding data, *Tectonophysics,* **420,** 239–252.

SUPPORTING INFORMATION

Supplementary data are available at *GJI* online.

Table S1. Thermal conductivity, thickness and thermal resistance of the reference discs.
Table S2. Global data on thermal conductivity for the sedimentary and metamorphic rocks are covered in this study.
Table S3. Global data on density for the sedimentary and metamorphic rocks are covered in this study.
Figure S1. Map showing distribution of heat flow in and around Himalayan Ranges (modified after Tunnini *et al.* 2016).
Figure S2. Calibration curve for conductivity meter QL-10.
Figure S3. Harker diagrams of sedimentary and metamorphic rocks, Western Himalaya, India.
Figure S4. Bivariate plots showing density (ρ) versus major oxides of sedimentary and the metamorphic rocks, Western Himalaya, India.
Data set D1: Major oxides (in weight per cent) of the sedimentary and the metamorphic rocks, Western Himalaya, India.
Data set D2: Saturated thermal conductivity (λ_{sat}), matrix thermal conductivity (λ_{mat}), density (ρ), porosity (ϕ) of the sedimentary and the metamorphic rocks, Western Himalaya, India.

Please note: Oxford University Press is not responsible for the content or functionality of any supporting materials supplied by the authors. Any queries (other than missing material) should be directed to the corresponding author for the paper.

APPENDIX

Geometric prediction model has been proposed by Lichtenecker (1926) and has been implemented by many researchers in geothermics (e.g. Woodside & Messmer 1961a,b; Popov *et al.* 2003; Fuchs *et al.* 2013). Study showed that for sedimentary rocks, this is the best among all other mathematical mean models.

The series distribution considers how the conductivity of a natural porous medium is represented by the intermediate weighted geometric mean:

$$\lambda_{eff} = \lambda_{Fluid}{}^{\phi} X \lambda_m{}^{1-\phi}.$$

The relationship between dry (λ_{dry}) and saturated (λ_{sat}) thermal conductivities can be written as

$$\lambda_{sat} = \lambda_w{}^{\phi} X \lambda_m{}^{1-\phi}, \quad \text{(A1)}$$

$$\lambda_{dry} = \lambda_{air}{}^{\phi} X \lambda_m{}^{1-\phi}, \quad \text{(A2)}$$

where, λ_m is matrix thermal conductivity and ϕ is porosity.